RSC Advances

ROYAL SOCIETY OF CHEMISTRY

www.rsc.org/advances

Journal Name

RSCPublishing

ARTICLE

Dynamic and Static Behavior of the E–E' Bonds (E, E' = S and Se) in Cystine and Derivatives, Elucidated by AIM Dual Functional Analysis†

Yutaka Tsubomoto, Satoko Hayashi and Waro Nakanishi*

Cite this: DOI: 10.1039/x0xx00000x

Received 00th October 2014,
Accepted 00th October 2014

DOI: 10.1039/x0xx00000x

www.rsc.org/

Atoms-in-molecules dual functional analysis (AIM-DFA) is applied to the E–E' bonds (E, E' = S and Se) in *R*-cystine (**1**) and the derivatives of **1**, together with MeEE'Me. $H_b(\boldsymbol{r}_c)$ are plotted versus $H_b(\boldsymbol{r}_c) - V_b(\boldsymbol{r}_c)/2$ at bond critical points (BCPs), where $H_b(\boldsymbol{r}_c) - V_b(\boldsymbol{r}_c)/2 = (\hbar^2/8m)\nabla^2\rho_b(\boldsymbol{r}_c)$. The plots are analyzed by the polar coordinate (R, θ) representation. Data of perturbed structures around the fully optimized structures are also plotted in this treatment. Perturbed structures are generated using NIV (normal coordinates of internal vibrations). Each plot for an interaction with data of a fully optimized and four perturbed structures gives a curve, which supplies important information. It is expressed by (θ_p, κ_p): θ_p corresponds to the tangent line for the plot measured from the y-direction and κ_p is the curvature. While (R, θ) correspond to the static nature of interactions, (θ_p, κ_p) represent the dynamic nature. The behavior of the E–E' bonds is well described by (R, θ) and (θ_p, κ_p).

Introduction

The E–E' bonds (E, E' = S and Se) are of current and continuous interest due to the indispensable role in biological, chemical and physical sciences.[1–7] The S–S bond plays a crucial role to maintain the three dimensional structures of peptides. On the other hand, the E–E' bonds show typical behavior in the redox process,[8] which must be responsible for the highly important biological activities such as detoxification of hydroperoxides in the glutathione peroxidase (GPx) process.[9–21]

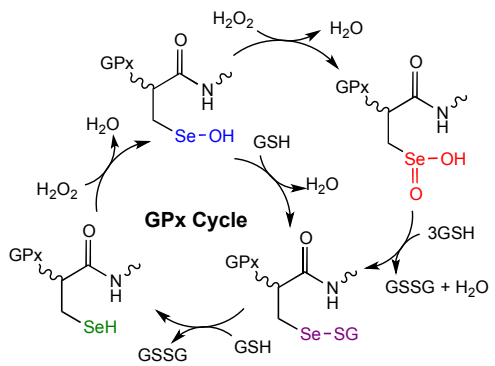

Scheme 1 Proposed Catalytic Mechanism for the Antioxidant Activity of GPx.

Scheme 1 summarizes the proposed catalytic mechanism for the antioxidant activity of GPx, which is one of typical examples of the intervention of E–E' in biological activities. The mechanism involves the initial oxidation of selenol (R_1-SeH) to produce the corresponding selenenic acid (R_1-SeOH), which reacts with glutathione (GSH) to produce selenenyl sulfide (R_1-SeSG). Then a second molecule of GSH attacks at the sulfur center of R_1-SeSG to regenerate the active form of the enzyme (R_1-SeH) (GPx cycle in Scheme 1). In the overall process, 2 equivalent of GSH is oxidized to the corresponding disulfide (GSSG), while the hydroperoxide is reduced to water.[22,23] When the peroxide concentration is higher than that of the thiol, the selenium center in the selenenic acid (R_1-SeOH) may undergo further oxidation to produce the seleninic acid (R_1-SeO_2H) (another cycle in Scheme 1).

The behavior of the E–E' bonds seems well described at first glance, however, it is still of highly importance to clarify the causality in the phenomena of the bonds, with physical necessity. Here, we clarified the dynamic and static behavior of the S–S bond in *R*-cystine (**1**), of which structures were determined by the X-ray crystallographic analysis, although the derivatives.[24] Similar behavior of the S–Se and Se–Se bonds in the derivatives of **1** (**2** and **3**, respectively) was also investigated, together with the E–E' bonds in MeEE'Me (E, E' = S and Se) (**4**–**6**, respectively) (Chart 1). The effect of the

hydrogen bonds (HBs) in **1**–**3** on the dynamic and static nature of the E–E' bonds must also be of interest.

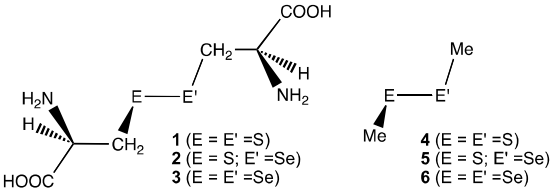

Chart 1 Chalcogen–chalcogen bonds in **1**–**6**, examined.

Atoms-in-molecules dual functional analysis (AIM-DFA),[25–28] which we proposed recently, is applied to the E–E' bonds in **1**–**6**. AIM-DFA is surveyed next, together with the basic concept of the AIM approach introduced by Bader.[29–31]

Survey of AIM and AIM Dual Functional Analysis

AIM (atoms-in-molecules method), proposed by Bader,[29–31] enables us to analyze and evaluate the nature of chemical bonds and interactions, together with the classification.[32–36] The bond critical point (BCP; $\boldsymbol{r}_c$, *) is an important concept in AIM. BCP of $(\omega, \sigma) = (3, -1)$[29,30] is a point along the bond path at the interatomic surface, where electron densities at BCPs ($\rho_b(\boldsymbol{r}_c)$) reaches a minimum. Chemical bond or interaction between A and B is denoted by A–B, which corresponds to the bond path between A and B in AIM. A notation A-*-B will be employed for A–B to emphasize the presence of BCP (*) in A–B.

Interactions are classified by signs of $\nabla^2\rho_b(\boldsymbol{r}_c)$ (Laplacian $\rho_b(\boldsymbol{r}_c)$) and $H_b(\boldsymbol{r}_c)$ (total electron energy densities). $H_b(\boldsymbol{r}_c)$ are the sum of kinetic energy densities ($G_b(\boldsymbol{r}_c)$) and potential energy densities ($V_b(\boldsymbol{r}_c)$) at BCPs, as shown in eqn (1). Eqn (2) represents the relation between $\nabla^2\rho_b(\boldsymbol{r}_c)$ and $H_b(\boldsymbol{r}_c)$, together with $G_b(\boldsymbol{r}_c)$ and/or $V_b(\boldsymbol{r}_c)$, which is closely related to the Virial theorem.

$$H_b(\boldsymbol{r}_c) = G_b(\boldsymbol{r}_c) + V_b(\boldsymbol{r}_c) \quad (1)$$

$$(\hbar^2/8m)\nabla^2\rho_b(\boldsymbol{r}_c) = H_b(\boldsymbol{r}_c) - V_b(\boldsymbol{r}_c)/2 \quad (2)$$

$$= G_b(\boldsymbol{r}_c) + V_b(\boldsymbol{r}_c)/2 \quad (2')$$

Interactions in the region of $\nabla^2\rho_b(\boldsymbol{r}_c) < 0$ are called shared-shell (SS) interactions and they are closed-shell (CS) interactions for $\nabla^2\rho_b(\boldsymbol{r}_c) > 0$. $H_b(\boldsymbol{r}_c)$ must be negative when $\nabla^2\rho_b(\boldsymbol{r}_c) < 0$, since $H_b(\boldsymbol{r}_c)$ are larger than $(\hbar^2/8m)\nabla^2\rho_b(\boldsymbol{r}_c)$ by $V_b(\boldsymbol{r}_c)/2$ with negative $V_b(\boldsymbol{r}_c)$ at all BCPs (eqn (2)). Consequently, $\nabla^2\rho_b(\boldsymbol{r}_c) < 0$ and $H_b(\boldsymbol{r}_c) < 0$ for the SS interactions. The CS interactions are especially called *pure* CS interactions for $H_b(\boldsymbol{r}_c) > 0$ and $\nabla^2\rho_b(\boldsymbol{r}_c) > 0$, since electrons are destabilized and $\rho(\boldsymbol{r})$ are depleted at (around) BCPs under the conditions.[29] Electrons in the intermediate region between SS and *pure* CS, which belong to CS, are locally depleted but stabilized at BCPs, since $\nabla^2\rho_b(\boldsymbol{r}_c) > 0$ but $H_b(\boldsymbol{r}_c) < 0$.[29] We call the interactions in this region *regular* CS,[25–27] when it is necessary to distinguish from *pure* CS. The role of $\nabla^2\rho_b(\boldsymbol{r}_c)$ in the classification can be replaced by $H_b(\boldsymbol{r}_c) - V_b(\boldsymbol{r}_c)/2$, since $(\hbar^2/8m)\nabla^2\rho_b(\boldsymbol{r}_c) = H_b(\boldsymbol{r}_c) - V_b(\boldsymbol{r}_c)/2$ (eqn (2)).

We proposed AIM-DFA by plotting $H_b(\boldsymbol{r}_c)$ versus $H_b(\boldsymbol{r}_c) - V_b(\boldsymbol{r}_c)/2$.[26,27] Both axes in the plot are given in energy unit, therefore, distances on the (x, y) [$= (H_b(\boldsymbol{r}_c) - V_b(\boldsymbol{r}_c)/2, H_b(\boldsymbol{r}_c))$] plane can be expressed in the energy unit, which provides an analytical development. AIM-DFA incorporates the classification of interactions by signs of $\nabla^2\rho_b(\boldsymbol{r}_c)$ [$= (8m/\hbar^2)(H_b(\boldsymbol{r}_c) - V_b(\boldsymbol{r}_c)/2)$] and $H_b(\boldsymbol{r}_c)$. Scheme 2 summarizes the treatment. Interactions of *pure* CS appear in the first quadrant, those of *regular* CS in the forth quadrant and data of the SS interactions drop in the third quadrant. No interactions appear in the second one.

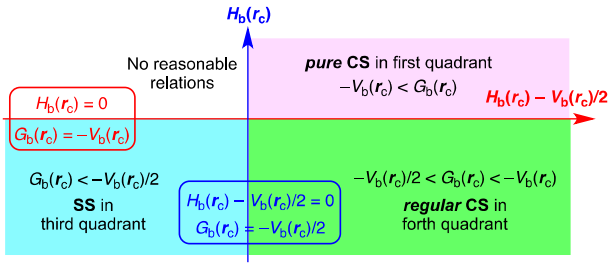

Scheme 2 AIM-DFA Treatment of Interactions: Plot of $H_b(\boldsymbol{r}_c)$ versus $H_b(\boldsymbol{r}_c) - V_b(\boldsymbol{r}_c)/2$ for Weak to Strong Interactions.

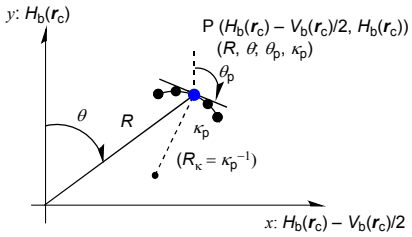

Fig. 1 Polar (R, θ) coordinate representation of $H_b(\boldsymbol{r}_c)$ versus $H_b(\boldsymbol{r}_c) - V_b(\boldsymbol{r}_c)/2$, with the (θ_p, κ_p) parameters.

$$R = (x^2 + y^2)^{1/2} \quad (3)$$

$$\theta = 90° - \tan^{-1}(y/x) \quad (4)$$

$$\theta_p = 90° - \tan^{-1}(dy/dx) \quad (5)$$

$$\kappa_p = |d^2y/dx^2| / [1 + (dy/dx)^2]^{3/2} \quad (6)$$

$$k = V_b(\boldsymbol{r}_c)/G_b(\boldsymbol{r}_c) \quad (7)$$

where $(x, y) = (H_b(\boldsymbol{r}_c) - V_b(\boldsymbol{r}_c)/2, H_b(\boldsymbol{r}_c))$
and $y/x = H_b(\boldsymbol{r}_c)/(H_b(\boldsymbol{r}_c) - V_b(\boldsymbol{r}_c)/2)$.

In our treatment, data for perturbed structures around fully optimized ones are also employed for the plots, together with the fully optimized structures.[25–28] The method to generate the perturbed structures will be discussed later. The plots of $H_b(\boldsymbol{r}_c)$ versus $H_b(\boldsymbol{r}_c) - V_b(\boldsymbol{r}_c)/2$ are analyzed employing the polar coordinate (R, θ) representation with the (θ_p, κ_p) parameters.[26–28] The treatment is explained in Fig. 1. R in (R, θ) is defined by eqn (3) and given in the energy unit. R corresponds to the energy for an interaction at BCP. The plots for weak to strong interactions show a spiral stream, as a whole. θ in (R, θ) is defined by eqn (4) and measured from the y-axis. θ controls the spiral stream of the whole plots. Each plot for an interaction shows a specific curve, which provides important

information.[26,27,37] The curve is expressed by (θ_p, κ_p). θ_p is defined by eqn (5) and measured from the *y*-direction, which corresponds to the tangent line of the plot. κ_p is the curvature of the plot (eqn (6)).[28] While (R, θ) correspond to the static nature of interactions, (θ_p, κ_p) represent the dynamic nature. Indeed, (θ_p, κ_p) originate mainly from the data of perturbed structures, but they are recognized as the nature at the fully optimized structure. k defined by eqn (7) is also an important and useful parameter in AIM analysis. AIM-DFA will provide an excellent possibility to evaluate, understand and classify weak to strong interactions in a unified form.

Methodological Details of QC and AIM Calculations

Structures of **1**–**6** were optimized using the Gaussian 09 program package,[38] after the conformation research with the Monte-Carlo method[39] in the Spartan 02[40] for **1**–**3**. Seven hundred and twenty two conformers were generated for each with the PM3 method.[41] Thirty of most stable conformers by the Monte-Carlo method were re-optimized using the 6-311+G(3d) basis sets[42] for S and Se and the 6-311++G(d, p) basis sets for O, N, C and H at the M062X level.[43] Frequency analysis was performed on three of most stable conformers at the same method for each of **1a**–**3c**, where **a** represents the most stable conformer with the second and third ones by **b** and **c**, respectively. The global minima for **4**–**6** were determined by usual optimizations with the frequency analysis.

AIM parameters were calculated with the Gaussian 09 program package and analyzed by the AIM2000 program.[44] Normal coordinates of the internal vibrations (NIV) are employed to generate the perturbed structures necessary to evaluate the dynamic nature of the interactions.[28] The k-th perturbed structures in question ($\mathbf{S}_{kw}$) will be given by the addition of the k-th NIV ($\mathbf{N}_k$) to the coordinates of the standard orientation at the fully optimized structure ($\mathbf{S}_o$) in the matrix representation.[28] Eqn (8) explains the treatment. The r(E, E') values in the perturbed structures were determined as shown by eqn (9) or (9'), where a_o is the Bohr radius (0.52918 Å). Data at w = 0, ±0.05 and ±0.1 were employed for the analysis.[26,27,45] The k-th internal vibration (ν_n) must be located most effectively on E–E', which corresponding to the selected $\mathbf{N}_k$.

$$\mathbf{S}_{kw} = \mathbf{S}_o + f_{kw} \bullet \mathbf{N}_k \quad (8)$$

$$r(\mathrm{E}, \mathrm{E}') = r_o(\mathrm{E}, \mathrm{E}') + wa_o \quad (9)$$

$$r = r_o + wa_o \quad (9')$$

Results and Discussion

Fig. 2 draws the three of most stable conformers for **1a**–**3c**. Fig. 2 also shows the stretching modes of **1a**–**3c**, necessary to evaluate the dynamic nature of the E–E' bonds with NIV. Conformers **1a**–**3c** are stabilized by intramolecular HBs, as shown in Fig. 2. Table 1 collects the optimized E–E' distances and torsional angles (ϕ(CEE'C)) for **1**–**6**, together with the distances and angles for the intramolecular HBs formed between the different moieties of the E–E' bonds in **1a**–**3c**.

Fig. 3 shows contour maps of $\rho_b(\boldsymbol{r}_c)$ drawn on an EE'C plane of **1a**–**3c**. All BCPs expected are clearly detected, containing those on the E–E', E–C (E'–C) and C–H bonds. AIM-DFA is applied to clarify the static and dynamic behavior of E–E' in **1**–**6**. Fig. 4 shows the plots of $H_b(\boldsymbol{r}_c)$ versus $H_b(\boldsymbol{r}_c) - V_b(\boldsymbol{r}_c)/2$ for **1**–**6**. The magnified picture around the data of the fully optimized structures for **2a**–**2c** and **5** is also shown in Fig. 4. AIM parameters corresponding to the static and dynamic behavior of E–E' are obtained for **1**–**6**, through analysis of the plots in Fig. 4, according to eqns (3)–(6). Table 2 collects the AIM functions and parameters of the static behavior evaluated

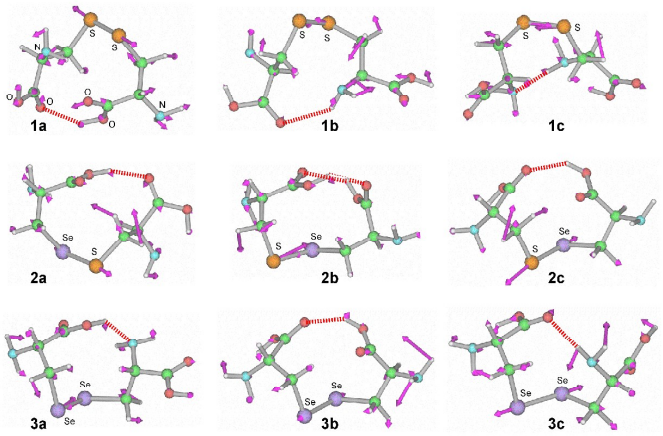

Fig. 2 Optimized structures for **1a**–**3c**. Directions of the motions, corresponding to NIV used to generate the perturbed structures, are shown (purple arrows), together with the intramolecular hydrogen bonds (red heavy dotted lines).

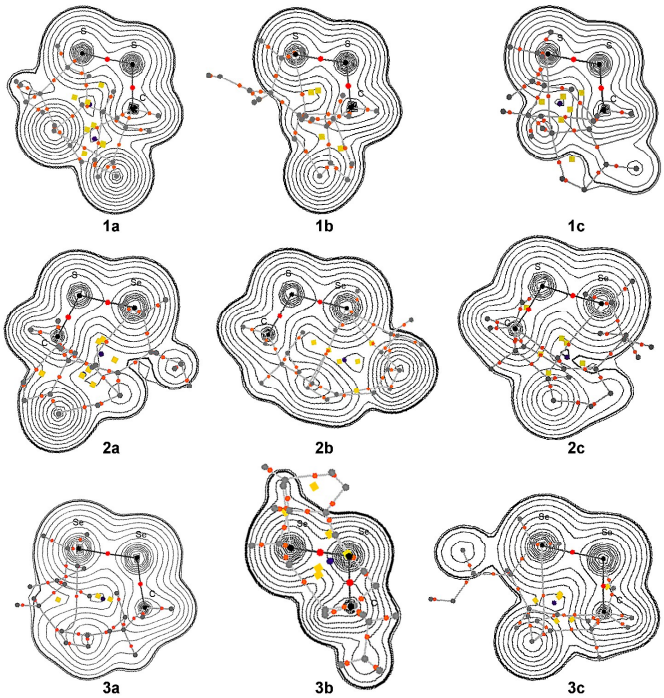

Fig. 3 Contour maps of $\rho_b(\boldsymbol{r}_c)$ drawn on the E–E'–C planes of **1a**–**3c**, together with BCPs (red solid circles), RCPs (ring critical points: lime green solid squares), and bond paths (solid lines). The counters (ea_o^{-3}) are at 2^l (l = ±8, ±7, ---, 0) and 0.0047, which corresponds to the molecular surface (heavy line).

Table 1 Optimized E–E' distances and torsional angles for **1**–**6**, together with the distances and angles for the intramolecular hydrogen bonds in **1a**–**3c**[a]

Species[b]	ΔE_{rel} (kJ mol^{-1})	r_o(E, E') (Å)	ϕ(CEE'C) (º)	(A–H---B)	r_o(A, H) (Å)	r_o(B, H) (Å)	∠AHB (º)
RS-*-SR (**1a**: C_1)	0.0	2.0625	67.7	(O–H---O)	0.9780	1.9828	149.8
RS-*-SR (**1b**: C_1)	0.3	2.0471	–82.2	(N–H---O)	1.0155	2.4136	134.4
RS-*-SR (**1c**: C_1)	0.7	2.0529	88.5	(N–H---N)	1.0210	2.2551	172.3
RS-*-SeR (**2a**: C_1)	0.0	2.1984	–83.9	(O–H---O)	0.9850	1.8025	156.4
RS-*-SeR (**2b**: C_1)	15.7	2.1890	84.3	(O–H---O)	0.9748	1.8996	142.6
				(O–H---O)	0.9743	2.1631	126.4
RS-*-SeR (**2c**: C_1)	17.5	2.2011	94.0	(O–H---O)	0.9771	1.8581	142.9
RSe-*-SeR (**3a**: C_1)	0.0	2.3275	88.5	(O–H---N)	0.9863	1.8955	137.7
RSe-*-SeR (**3b**: C_1)	1.4	2.3303	93.4	(O–H---O)	0.9773	1.8335	145.1
RSe-*-SeR (**3c**: C_1)	3.3	2.3309	90.2	(N–H---O)	1.0193	2.0185	167.6
MeS-*-SMe (**4**: C_2)		2.0491	85.0				
MeSe-*-SMe (**5**: C_1)		2.1923	85.6				
MeSe-*-SeMe (**6**: C_2)		2.3236	86.1				

[a] The 6-311+G(3d) basis sets being employed for S and Se with the 6-311++G(d,p) basis sets for O, N, C and H at the DFT level of M06-2X. [b] RSH = *R*-cysteine.

Table 2 Static nature of the E–E' bonds in **1**–**6** at full optimized structures[a]

Species[b]	$\rho_b(\boldsymbol{r}_c)$ (au)	$c\nabla^2\rho_b(\boldsymbol{r}_c)^c$ (au)	$H_b(\boldsymbol{r}_c)$ (au)	R^d (au)	θ^e (º)	k^f
RS-*-SR (**1a**: C_1)	0.1409	–0.0117	–0.0710	0.0719	189.4	–2.495
RS-*-SR (**1b**: C_1)	0.1443	–0.0126	–0.0749	0.0759	189.6	–2.509
RS-*-SR (**1c**: C_1)	0.1432	–0.0124	–0.0737	0.0747	189.6	–2.508
RS-*-SeR (**2a**: C_1)	0.1171	–0.0041	–0.0529	0.0531	184.4	–2.183
RS-*-SeR (**2b**: C_1)	0.1188	–0.0045	–0.0547	0.0548	184.7	–2.195
RS-*-SeR (**2c**: C_1)	0.1166	–0.0040	–0.0525	0.0527	184.4	–2.180
RSe-*-SeR (**3a**: C_1)	0.1020	–0.0042	–0.0431	0.0433	185.6	–2.242
RSe-*-SeR (**3b**: C_1)	0.1021	–0.0046	–0.0432	0.0434	186.0	–2.268
RSe-*-SeR (**3c**: C_1)	0.1023	–0.0046	–0.0435	0.0437	186.1	–2.269
MeS-*-SMe (**4**: C_2)	0.1446	–0.0131	–0.0751	0.0763	189.9	–2.535
MeSe-*-SMe (**5**: C_1)	0.1189	–0.0048	–0.0544	0.0547	185.0	–2.213
MeSe-*-SeMe (**6**: C_2)	0.1036	–0.0050	–0.0445	0.0448	186.4	–2.291

[a] The 6-311+G(3d) basis sets being employed for S and Se with the 6-311++G(d,p) basis sets for O, N, C and H at the DFT level of M06-2X. [b] RSH = *R*-cysteine. [c] $c\nabla^2\rho_b(\boldsymbol{r}_c) = H_b(\boldsymbol{r}_c) - V_b(\boldsymbol{r}_c)/2$ where $c = \hbar^2/8m$. [d] $R = [(H_b(\boldsymbol{r}_c) - V_b(\boldsymbol{r}_c)/2)^2 + H_b(\boldsymbol{r}_c)^2]^{1/2}$ (eqn (3)). [e] $\theta = 90º - \tan^{-1}[H_b(\boldsymbol{r}_c)/(H_b(\boldsymbol{r}_c) - V_b(\boldsymbol{r}_c)/2)]$ (eqn (4)). [f] $k = V_b(\boldsymbol{r}_c)/G_b(\boldsymbol{r}_c)$ (eqn (7)).

Table 3 Dynamic Nature of the E–E' Bonds in **1**–**6** with NIV[a]

Species[b]	$\nu_n{}^c$ (cm^{-1})	n for ν_n	$k_f{}^d$ (mdyn Å^{-1})	$\theta_p{}^e$ (º)	$\kappa_p{}^f$ (au^{-1})
RS-*-SR (**1a**: C_1)	511.3	20	2.060	197.5	0.75
RS-*-SR (**1b**: C_1)	522.5	21	1.118	197.4	0.67
RS-*-SR (**1c**: C_1)	506.8	20	1.947	197.5	0.69
RS-*-SeR (**2a**: C_1)	414.4	18	0.551	188.0	0.34
RS-*-SeR (**2b**: C_1)	423.6	19	1.896	188.4	0.33
RS-*-SeR (**2c**: C_1)	414.7	19	1.440	188.2	0.40
RSe-*-SeR (**3a**: C_1)	301.9	15	1.875	188.9	0.71
RSe-*-SeR (**3b**: C_1)	308.0	16	0.174	189.3	0.77
RSe-*-SeR (**3c**: C_1)	298.7	13	0.938	189.4	0.68
MeS-*-SMe (**4**: C_2)	513.7	6	2.645	197.6	0.66
MeS-*-SeMe (**5**: C_1)	419.7	6	2.072	188.6	0.38
MeSe-*-SeMe (**6**: C_2)	307.7	6	2.730	189.1	0.77

[a] The 6-311+G(3d) basis sets being employed for S and Se with the 6-311++G(d,p) basis sets for O, N, C and H at the DFT level of M062X. [b] RSH = *R*-cysteine. [c] Frequency corresponding to the stretching mode of the E-*-E' bond, where * means the bond critical point in question. [d] Force constants correspond to ν_n. [e] $\theta_p = 90º - \tan^{-1}(dy/dx)$ where $(x, y) = (H_b(\boldsymbol{r}_c) - V_b(\boldsymbol{r}_c)/2, H_b(\boldsymbol{r}_c))$ (eqn (5)). [f] $k_p = |d^2y/dx^2|/[1 + (dy/dx)^2]^{3/2}$ (eqn (6)).

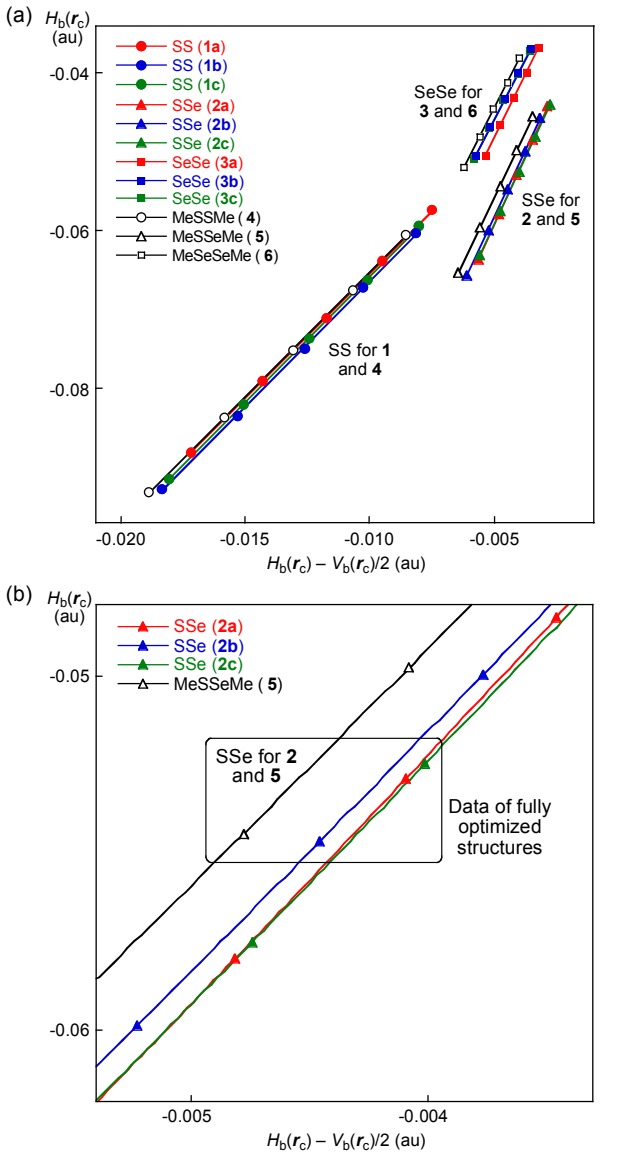

Fig. 4 Plots of $H_b(r_c)$ versus $H_b(r_c) - V_b(r_c)/2$ for **1**–**6**. (a) Whole picture and (b) magnified one around data of fully optimized structures for **2a**–**2c** and **5**.

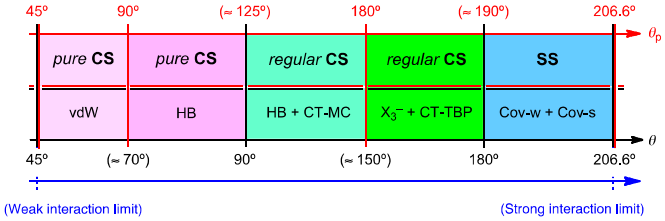

Scheme 3 Rough classification of Interactions by θ and θ_p.

for **1**–**6**. Table 3 summarizes the AIM parameters of the dynamic behavior evaluated for **1**–**6**.

The behavior of E–E' in **1**–**6** is examined by comparing the (θ, θ_p, R) values with those of the standard ones. The standard values are roughly determined to classify the interactions in question, employing typical weak to strong interactions. Scheme 3 illustrates the standard values for the typical interactions. The results tell us that θ are larger than 180º for SS interactions, which correspond to $H_b(r_c) - V_b(r_c)/2 < 0$. The θ_p value will play an important role to discuss the characters of CS interactions with $\theta < 180º$ ($H_b(r_c) - V_b(r_c)/2 > 0$). While the character of interactions will be that of CT-TBP (trigonal bipyramidal adducts formed through charge-transfer) such as in $Me_2Se(-*-Cl)_2$, if $\theta_p > 180º$, it will be that of CT-MC (molecular complexes formed through CT) such as in $Me_2S-*-Br_2$, when $\theta_p < 180º$, for example. The R values contribute to classify SS, further. Classical chemical bonds of SS are strong for $R > 0.15$ au but they would be weak when $R < 0.15$ au.[26]

The (θ/º, θ_p/º, R/au) values for S–S in **1a** and **4** are (189.4, 197.5, 0.072) and (189.9, 197.6, 0.076), respectively. While the values for S–Se in **2a** and **5** are (184.4, 188.0, 0.053) and (185.0, 188.6, 0.055), respectively, those for Se–Se in **3a** and **6** are (185.6, 188.9, 0.043) and (186.4, 189.1, 0.045), respectively. The results show that all E–E' in **1**–**6** are classified as the weak covalent bonds, since $\theta > 180º$ with $R < 0.15$ au.[26] The nature of E–E' in **1a**–**3a** is predicted to be very close to that of **4**–**6**, respectively. The strength of E–E' is reconfirmed in the order of Se–Se ≤ S–Se < S–S. All data of Se–Se, S–Se and S–S in **1**–**6** appear in the SS region. However, those of Se–Se and S–Se are closer to the *regular* CS region ($\theta_p \approx 189º$), relative to the case of S–S ($\theta_p \approx 198º$). Whereas R for **1a**–**3a** are less than those of **4**–**6**, respectively, the data for **1a**–**3a** seem to appear at the opposite side of the origin in the plots. The discrepancies must be the reflection of the complex contributions from $G_b(r_c)$ and $V_b(r_c)$ to $H_b(r_c)$ and $H_b(r_c) - V_b(r_c)/2$ in E-E', according to eqns (1) and (2). It would be difficult to specify the reason for the characteristic behaviour in the plots, based on the data in Tables 2 and 3.

How are the E–E' bonds affected by the formation of HBs? The formation of intramolecular HBs stabilizes **1**–**3**, relative to the conformers with no such interactions. The A–H---B angles are predicted to be around 130–150º for HBs in **1**–**3**, which must be the reflection of the restricted HBs in **1**–**3**. The results may suggest that the intramolecular HBs are formed under somewhat undesirable conditions (see Table 1). The HBs in **1**–**3** must affect on the stability and the strength of E–E' in **1**–**3**. The variation of ϕ(CEE'C) in **1**–**3**, relative to the case of **4**–**6**, must be another evidence for the restricted HBs (Table 1). The conformation also affect on the strength of E–E'. In the case of **2**, the S–Se bond becomes stronger in the order of **2c** ≤ **2a** < **2b**, although very slightly (see Fig. 4b). The strength of S–Se seems almost independent of the stability in **2a**–**c**, for example. Namely, such molecules are stabilized through the formation of HBs, but the E–E' bonds could be sacrificed and somewhat weakened by the distortion.

The nature of the E–E' bonds in **1**–**6** is well described with the dynamic nature of (θ_p, κ_p) and the static nature of (R, θ) by applying AIM-DFA.

Conclusion

AIM-DFA is applied to the E–E' bonds (E, E' = S and Se) in *R*-cystine (**1**) and the derivatives (**2** and **3** for the S–Se and Se–Se derivatives, respectively), together with those of MeEE'Me (**4**–**6**). The dynamic and static behavior is clarified for E–E' in **4**–**6** by the application. The nature of E–E' in **1**–**6** is further examined by comparing the (θ, $\theta_{\square}$, R) values with those of the standard ones. The (θ/º, $\theta_{\square}$/º, R/au) values for S–S in **1a** and **4** are (189.4, 197.5, 0.072) and (189.9, 197.6, 0.076), respectively. While the values for S–Se in **2a** and **5** are (184.4, 188.0, 0.053) and (185.0, 188.6, 0.055), respectively, those for Se–Se in **3a** and **6** are (185.6, 188.9, 0.043) and (186.4, 189.1, 0.045), respectively. All E–E' in **1**–**6** are classified as the weak covalent bonds. The nature of E–E' in **1a**–**3a** is very close to that in **4**–**6**, respectively. The strength of the bonds is predicted to be in the order of S–S > S–Se ≥ Se–Se. All data of E–E' in **1**–**6** appear in the SS region. However, those of Se–Se and S–Se are closer to the *regular* CS region ($\theta_{\square} \approx 189$º), relative to the case of S–S ($\theta_{\square} \approx 198$º). The A–H---B angles in HBs of **1**–**3** are predicted to be around 130–150º, which must be the reflection of the restricted HBs in **1**–**3**. Indeed, **1**–**3** are stabilized by the formation of HBs, but the E–E' bonds could be sacrificed and somewhat weakened by the distortion. The nature of the E–E' bonds in **1**–**6** is well described by (θ_p, κ_p) of the dynamic nature and (R, θ) of the static nature obtained through AIM-DFA.

Acknowledgements

This work was partially supported by a Grant-in-Aid for Scientific Research (Nos. 23350019 and 26410050) from the Ministry of Education, Culture, Sports, Science and Technology, Japan. The support of the Wakayama University Original Research Support Project Grant and the Wakayama University Graduate School Project Research Grant is also acknowledged.

Notes and references

Department of Material Science and Chemistry, Faculty of Systems Engineering, Wakayama University, 930 Sakaedani, Wakayama 640-8510, Japan. Fax: +81 73 457 8253; Tel: +81 73 457 8252; E-mail: nakanisi@sys.wakayama-u.ac.jp

† Electronic Supplementary Information (ESI) available: The fully optimized structures given by Cartesian coordinates for examined molecules and adducts. See DOI: 10.1039/b000000x/

1 (a) *Their Chemistry and Biology*, eds. D. L. Klayman and W. H. H. Günther, Wiley: New York, 1973; (b) *The Chemistry of Organic Selenium and Tellurium Compounds*, eds. S. Patai and Z. Rappoport, John-Wiley and Sons: New York, 1986; Vols. 1 and 2; (c) *Organic Selenium Chemistry*, ed. D. Liotta, Wiley-Interscience: New York, 1987; (d) *Organoselenium Chemistry, A practical Approach*, ed. T. G. Back, Oxford University Press: Oxford, 1999; (e) *Organoselenium Chemistry Modern Developments in Organic Synthesis, Top. Curr. Chem.*, ed. T. Wirth, Springer: Berlin, Heidelberg, New York, London, Paris, Tokyo, 2000.

2 *Chemistry of Hypervalent Compounds*, ed. K.-y. Akiba, Wiley-VCH, New York, 1999.

3 (a) W. Nakanishi, *Hypervalent Chalcogen Compounds* In *Handbook of Chalcogen Chemistry: New Perspectives in Sulfur, Selenium and Tellurium*, ed. F. A. Devillanova, Royal Society of Chemistry, Cambridge, 2006, ch. 10.3, pp 644–668; (b) W. Nakanishi and S. Hayashi, *Hypervalent Chalcogen Compounds* In *Handbook of Chalcogen Chemistry: New Perspectives in Sulfur, Selenium and Tellurium, 2nd Edition, Vol. 2*, eds. F. A. Devillanova and W.-W. du Mont, Royal Society of Chemistry, Cambridge, 2013, ch. 12.3, pp 335–372.

4 A. J. Mukherjee, S. S. Zade, H. B. Singh and R. B. Sunoj, *Chem. Rev.*, 2010, **110**, 4357.

5 M. Kulcsar, A. Beleaga, C. Silvestru, A. Nicolescu, C. Deleanu, C. Todasca and A. Silvestru, *Dalton Trans.*, 2007, 2187; A. Beleaga, M. Kulcsar, C. Deleanu, A. Nicolescu, C. Silvestru and A. Silvestru, *J. Organomet. Chem.*, 2009, **694**, 1308.

6 S. Hayashi and Nakanishi, W. *J. Org. Chem.,* 1999, **64**, 6688; W. Nakanishi, S. Hayashi and S. Toyota, *J. Org. Chem.*, 1998, **63**, 8790; W. Nakanishi, S. Hayashi and S. Toyota, *Chem. Commun.*, 1996, 371; W. Nakanishi, S. Hayashi and H. Yamaguchi, *Chem. Lett.*, 1996, 947; W. Nakanishi, *Chem. Lett.*, 1993, 2121.

7 W. Nakanishi, S. Hayashi and T. Arai, *Chem. Commun.,* 2002, 2416.

8 W. Nakanishi, S. Hayashi, S. Morinaka, T. Sasamori and N. Tokitoh, *New J. Chem.*, 2008, **32**, 1881.

9 (a) W. Brandt and L. A. Wessjohann, *Chem. Bio. Chem.*, 2005, **6**, 386; (b) S. Gromer and L. A. Wessjohann, J. Eubel and W. Brandt, *Chem. Bio. Chem.*, 2006, **7**, 1649; (c) L. A. Wessjohann, A. Schneider, M. Abbas and W. Brandt, *Biol. Chem.*, 2007, **388**, 997; (d) B. M. Lacey, B. E. Eckenroth, S, Flemer, Jr. and R. J. Hondal, *Biochemistry*, 2008, **47**, 12810; (e) L. A. Wessjohann and A. Schneider, *Chem. Biodiversity*, 2008, **5**, 375.

10 B. Ren, W. Huang, B. Åkesson and R. Ladenstein, *J. Mol. Biol.*, 1997, **268**, 869.

11 W. A. Hendrickson, *Science*, 1991, **254**, 51.

12 A. Ishii, S. Matsubayashi, T. Takahashi and J. Nakayama, *J. Org. Chem.*, 1999, **64**, 1084.

13 T. Saiki, K. Goto and R. Okazaki, *Angew. Chem., Int. Ed.*, 1997, **36**, 2223; K. Goto, D. Sonoda, K. Shimada, S. Sase and T. Kawashima, *Angew. Chem. Int. Ed.*, 2010, **49**, 545.

14 G. Mugesh and H. B. Singh, *Chem. Soc. Rev.*, 2000, **29**, 347.

15 K. P. Bhabak and G. Mugesh, *Chem. Asian J.*, 2009, **4**, 974; B. K. Sarma and G. Mugesh, *Chem. Eur. J.*, 2008, **14**, 10603.

16 K. P. Bhabak and G. Mugesh, *Chem. Eur. J.*, 2009, **15**, 9846; K. P. Bhabak and G. Mugesh, *Chem. Eur. J.*, 2008, **14**, 8640; K. P. Bhabak and G. Mugesh, *Chem. Eur. J.*, 2007, **13**, 4594; B. K. Sarma and G. Mugesh, *Inorg. Chem.*, 2006, **45**, 5307; P. P. Phadnis and G. Mugesh, *Org. Biomol. Chem.*, 2005, **3**, 2476.

17 M. Iwaoka, R. Ooka, T. Nakazato, S. Yoshida and S. Oishi, *Chem. Biodiv.*, 2008, **5**, 359.

18 F. Kumakura, B. Mishra, K. I. Priyadarsini and M. Iwaoka, *Eur. J. Org. Chem.*, 2010, 440.

19 K. Arai, K. Dedachi and M. Iwaoka, *Chem. Eur. J.*, 2011, **17**, 481.

20 S. Yoshida, F. Kumakura, I. Komatsu, K. Arai, Y. Onuma, H. Hojo, B. G. Singh, K. I. Priyadarsini and M. Iwaoka, *Angew. Chem. Int. Ed.*, 2011, **50**, 2125; *Angew. Chem.*, 2011, **123**, 2173.
21 D. Manna and G. Mugesh, *J. Am. Chem. Soc.*, 2012, **134**, 4269.
22 L. Flohé, E. A. Günzler and H. H. Schock, *FEBS Lett.,* 1973, **32**, 132.
23 L. Flohé, *Glutathione peroxidase brought into focus,* In *Free radicals in biology,* ed. W. A. Pryor, Academic Press, New York, 1982, Vol. 5, pp 223–253.
24 V. S. Minkov and E. V. Boldyreva, *Acta Crystallogr., Sect. C: Cryst. Struct. Commun.,* 2009, **65**, o245; T. N. Drebushchak, S. V. Bizyaev and E. V. Boldyreva, *Acta Crystallogr., Sect. C: Cryst. Struct. Commun.*, 2008, **64**, o313; V. S. Minkov and E. V. Boldyreva, *Acta Crystallogr., Sect. C: Cryst. Struct. Commun.*, 2008, **64**, o344.
25 W. Nakanishi, S. Hayashi and K. Narahara, *J. Phys. Chem. A*, 2008, **112**, 13593.
26 W. Nakanishi, S. Hayashi and K. Narahara, *J. Phys. Chem. A*, 2009, **113**, 10050.
27 W. Nakanishi and S. Hayashi, *Current Organic Chemistry,* 2010, **14**, 181.
28 W. Nakanishi and S. Hayashi, *J. Phys. Chem. A*, 2010, **114**, 7423.
29 *Atoms in Molecules. A Quantum Theory*, ed. R. F. W. Bader, Oxford University Press, Oxford, 1990.
30 *The Quantum Theory of Atoms in Molecules: From Solid State to DNA and Drug Design*, eds. C. F. Matta and R. J. Boyd, Wily-VCH, Weinheim, Germany, 2007, ch. 1.
31 (a) F. Biegler-König and J. Schönbohm, *J. Comput. Chem.*, 2002, **23**, 1489; (b) F. Biegler-König, J. Schönbohm and D. Bayles, *J. Comput. Chem*., 2001, **22**, 545; (c) R. F. W. Bader, *J. Phys. Chem. A*, 1998, **102**, 7314; (d) R. F. W. Bader, *Chem. Rev*., 1991, **91**, 893; (e) R. F. W. Bader, *Acc. Chem. Res*., 1985, **18**, 9; (f) T. H. Tang, R. F. W. Bader and P. MacDougall, *Inorg. Chem*., 1985, **24**, 2047; (g) R. F. W. Bader, T. S. Slee, D. Cremer and E. Kraka, *J. Am. Chem. Soc*., 1983, **105**, 5061; (h) F. Biegler-König, R. F. W. Bader and T. H. Tang, *J. Comput. Chem.*, 1982, **3**, 317.
32 J. M. Molina and J. A. Dobado, *Theor. Chem. Acc.*, 2001, **105**, 328.
33 J. A. Dobado, H. Martînez-Garcîa, J. M. Molina and M. R. Sundberg, *J. Am. Chem. Soc*., 2000, **122**, 1144.
34 S. K. Ignatov, N. H. Rees, B. R. Tyrrell, S. R. Dubberley, A. G. Razuvaev, P. Mountford and G. I. Nikonov, *Chem. Eur. J.*, 2004, **10**, 4991.
35 S. K. Tripathi, U. Patel, D. Roy, R. B. Sunoj, H. B. Singh, G. Wolmershäuser and R. J. Butcher, *J. Org. Chem.,* 2005, **70**, 9237.
36 Boyd, R.J.; Choi, S.C. *Chem. Phys. Lett.*, **1986**, *129*, 62.
37 See Fig. 2 in W. Nakanishi and S. Hayashi, *J. Phys. Chem. A*, 2013, **117**, 1795.
38 Gaussian 09, Revision D.01, M. J. Frisch, G. W. Trucks, H. B. Schlegel, G. E. Scuseria, M. A. Robb, J. R. Cheeseman, G. Scalmani, V. Barone, B. Mennucci, G. A. Petersson, H. Nakatsuji, M. Caricato, X. Li, H. P. Hratchian, A. F. Izmaylov, J. Bloino, G. Zheng, J. L. Sonnenberg, M. Hada, M. Ehara, K. Toyota, R. Fukuda, J. Hasegawa, M. Ishida, T. Nakajima, Y. Honda, O. Kitao, H. Nakai, T. Vreven, J. A. Montgomery, Jr., J. E. Peralta, F. Ogliaro, M. Bearpark, J. J. Heyd, E. Brothers, K. N. Kudin, V. N. Staroverov, R. Kobayashi, J. Normand, K. Raghavachari, A. Rendell, J. C. Burant, S. S. Iyengar, J. Tomasi, M. Cossi, N. Rega, J. M. Millam, M. Klene, J. E. Knox, J. B. Cross, V. Bakken, C. Adamo, J. Jaramillo, R. Gomperts, R. E. Stratmann, O. Yazyev, A. J. Austin, R. Cammi, C. Pomelli, J. W. Ochterski, R. L. Martin, K. Morokuma, V. G. Zakrzewski, G. A. Voth, P. Salvador, J. J. Dannenberg, S. Dapprich, A. D. Daniels, Ö. Farkas, J. B. Foresman, J. V. Ortiz, J. Cioslowski and D. J. Fox, Gaussian, Inc., Wallingford CT, 2009.
39 R. W. B. Ardill, K. J. M. Moriarty and M. Creutz, *Comput. Phys. Commun.*, 1983, **29**, 97; M. Creutz, *Phys. Rev. Lett.*, 1983, **50**, 1411, see also P. Bratley, B. L. Fox and L. E. Schrage. *A Guide to Simulation,* Springer-Verlag, New York, 1987; G. M. Kalos and P. A. Whitlock, *Monte Carlo Methods,* John Wiley & Sons, New York, 1986; A. R. Leach. *Molecular Modelling. Principles and Applications,* Addison Wesley Longman, Essex, England, 1996.
40 Spartan '02 for Windows, Wavefunction, Inc., Irvine, CA; *Spartan '02 Windows, Tutorial and User's Guide*, Wavefunction, Inc., Irvine CA, 2001.
41 J. J. P. Stewart, *J. Comp. Chem.,* 1989, **10**, 209.
42 In our experience, the 6-311+G(d) basis sets or higher ones are recommended, when usual organic selenium compounds are calculated. For the 6-311+G(3d) basis sets, see: R. C. Binning, Jr. and L. A. Curtiss, *J. Comput. Chem.*, 1990, **11**, 1206; L. A. Curtiss, M. P. McGrath, J.-P. Blaudeau, N. E. Davis, R. C. Binning, Jr. and L. Radom, *J. Chem. Phys.*, 1995, **103**, 6104; M. P. McGrath and L. Radom, *J. Chem. Phys.*, 1991, **94**, 511; for the diffuse functions (+ and ++), see T. Clark, J. Chandrasekhar, G. W. Spitznagel and P. v. R. Schleyer, *J. Comput. Chem.*, 1983, **4**, 294. See for example, W. Nakanishi, S. Hayashi, *J. Phys. Chem. A*, 1999, **103**, 6074.
43 Y. Zhao and G. D. Truhlar, *Org. Lett*., 2006, **8**, 5753; E. S. Wheeler and N. K. Houk, *J. Chem. Theory Comput.,* 2010, **6**, 395; S. Rayne and K. Forest, *J. Mol. Struct.:THEOCHEM*, 2010, **948**, 102; S. Rayne and K. Forest, *Nature Precedings*, 2010, doi:10.1038/npre.2010.4865.1.
44 The AIM2000 program (Version 2.0) is employed to analyze and visualize atoms in molecules: F. Biegler-König, *J. Comput. Chem.*, 2000, **21**, 1040; see also ref. 31b.
45 The bond orders become 1.50 and 0.67 times larger than the initial value if they are calculated at $0.2a_o$ shorter and longer distances from the initial length, respectively.[46] The change in the length could be observed and seems to affect not so much on our discussion to classify the weak interactions.
46 Pauling, L. *The Nature of the Chemical Bond*, 3rd ed., Cornell University Press, Ithaca, New York, **1960**, Chap. 7, pp. 221–264; Pauling, L. *J. Am. Chem. Soc.*, **1947**, *69*, 542.

Graphical contents entry:

AIM-DFA (atoms-in-molecules dual functional analysis) is applied to the E–E' bonds (E, E' = S and Se) in *R*-cystine (**1**) and the derivatives, together with MeEE'Me. The nature of E–E' is elucidated by the dynamic behaviour with (θ_p, κ_p) and the static behavior with (R, θ), through AIM-DFA.

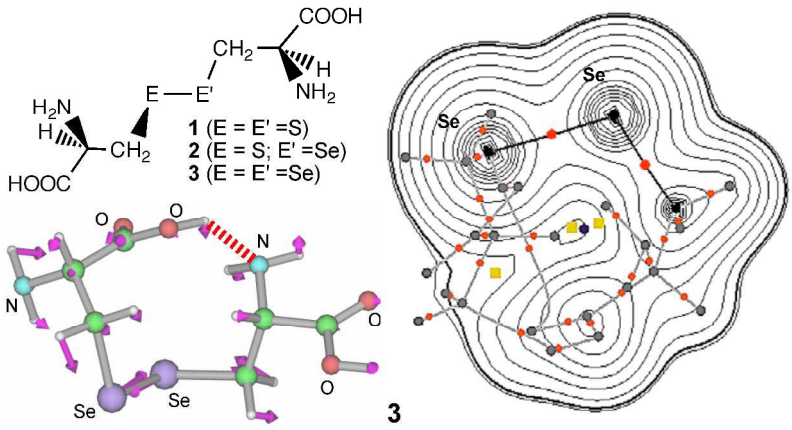

Keywords:

ab initio calculations, AIM dual functional analysis, atoms-in-molecules, chalcogen-chalcogen bonds, cystine